SoRo

Soft Robotics

Open camera or QR reader and
scan code to access this article
and other resources online.

Multifunctional Soft Stackable Robots by Netting–Rolling–Splicing Pneumatic Artificial Muscles

Qinghua Guan,[1] Liwu Liu,[2] Jian Sun,[1] Jiale Wang,[2] Jianglong Guo,[3] Yanju Liu,[2] and Jinsong Leng[1]

Abstract

Soft robots equipped with multifunctionalities have been increasingly needed for secure, adaptive, and autonomous functioning in unknown and unpredictable environments. Robotic stacking is a promising solution to increase the functional diversity of soft robots, which are required for safe human–machine interactions and adapting in unstructured environments. However, most existing multifunctional soft robots have a limited number of functions or have not fully shown the superiority of the robotic stacking method. In this study, we present a novel robotic stacking strategy, Netting–Rolling–Splicing (NRS) stacking, based on a dimensional raising method via 2D-to-3D rolling-and-splicing of netted stackable pneumatic artificial muscles to quickly and efficiently fabricate multifunctional soft robots based on the same, simple, and cost-effective elements. To demonstrate it, we developed a TriUnit robot that can crawl 0.46 ± 0.022 body length per second (BL/s) and climb 0.11 BL/s, and can carry a 3 kg payload while climbing. Also, the TriUnit can be used to achieve novel omnidirectional pipe climbing including rotating climbing, and conduct bionic swallowing-and-regurgitating, multidegree-of-freedom manipulation based on their multimodal combinations. Apart from these, steady rolling, with a speed of 0.19 BL/s, can be achieved by using a pentagon unit. Furthermore, we applied the TriUnit pipe climbing robot in panoramic shooting and cargo transferring to demonstrate the robot's adaptability for different tasks. The NRS stacking-driven soft robot here has demonstrated the best overall performance among existing stackable soft robots, representing a new and effective way for building multifunctional and multimodal soft robots in a cost-effective and efficient way.

Keywords: multifunctional, multimodal, modular, pneumatic artificial muscles, soft stackable robots

Introduction

MULTIFUNCTION IS AN essential ability of robots so that they can complete tasks in different conditions and adapt in unstructured environments. Soft mobile robots, compared with their rigid counterparts, have better environmental adaptability, safer human–machine–environment interactions, and increased compliance, and are thus more suitable for multimodal locomotion and performing dexterous, delicate manipulation tasks.[1] Various engineering solutions to multifunctional soft mobile robots have been developed. For example, Hu *et al.* developed a magnetically

[1]Centre for Composite Materials and Structures, Harbin Institute of Technology (HIT), Harbin, People's Republic of China.
[2]Department of Astronautical Science and Mechanics, Harbin Institute of Technology (HIT), Harbin, People's Republic of China.
[3]School of Science, Harbin Institute of Technology (Shenzhen), Shenzhen, People's Republic of China.
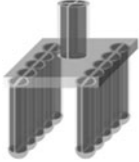
driven soft mobile robot that can swim, climb, roll, walk, jump, crawl, and conduct material handling tasks, although a customized external magnetic field and specialized magnetization profiles are required.[2] Robotic stacking is an appealing solution to multifunctional robots. For instance, Robertson and Paik demonstrated a series of vacuum-driven soft modular robots that are capable of crawling, rolling, and climbing and can execute material handling and active stiffness tuning tasks.[3]

Here, we categorize existing robotic stacking mechanisms into 0D, 1D, 2D, and 3D ones, as summarized in Table 1. 0D stacking relies on one connection joint to fix all actuators together with a hub-and-spoke arrangement.[4–10] In 1D stacking, actuators are connected by joining ends in series[11–15] or parallel.[16] In 2D stacking, actuators are connected to each other in planar structures.[17–22] In 3D stacking, actuators are stacked into 3D structures such as brick piling,[23,24] space frame,[25] and tensegrity[26] ones. Different stacking mechanisms can also be combined together to create robotic structures with more functions such as "1D+0D,"[27,28] "2D+0D,"[29] "2D+1D."[3,30,31] However, most existing stacking strategies extended their capabilities by only increasing their stacking dimensions, which has limited the integration of some novel functions and cannot fully show the superiority of the robotic stacking method.

Robertson and Paik also integrated crawling, climbing, rolling, and manipulation into a series of soft modular robots.[3] Here, in our study, not only the swallowing/storing/

TABLE 1. SUMMARY OF COMMON ROBOTIC STACKING MECHANISMS

Stacking dimensions	Diagrams	Crawling	Climbing	Rolling	Swallow Enveloping gripping	Swallow Inner-though transportation	Manipulation
0D		√ 4–6		√ 7,8	√ 9,10		
1D		√ 11,15	√ 12,15		√ 13		√ 13,14,16
2D		√ 17			√ 18,22		√ 19–21
3D		√ 23		√ 25,26			√ 24
Combinations							
1D+0D		√ 27,28					
2D+0D					√ 29		√ 29
2D+1D		√ 3	√ 3	√ 3			√ 3,30,31
This work 2D Netting+Rolling and Splicing		√	√	√	√	√	√

disgorging behaviors were realized, but also other locomotion forms were investigated such as mono-oscillation crawling, out-pipe/inner-pipe climbing, rotating–climbing, and swallowing–storing manipulation. Also, there is a lack of multifunctional soft robots that couple the swallowing/disgorging function, which is quite common in nature, to enhance their versatility, although there are several published studies on enveloping gripping[32,33] and inner-though transporting.[34–36] For example, Wang *et al.* showed the simulated swallowing and disgorging process using a hydraulic artificial muscle-driven manipulator for underwater applications based on three rigid linked planar linkages.[37] Zhang *et al.* proposed a swallowing robot actuated axially and sectionally based on Hoberman's linkages.[38] However, their limited flexibility may inhibit the adaptability and versatility of their robots.

Pneumatic artificial muscles (PAMs) have excellent compliance and large output forces and displacements with decent robustness. They have, therefore, been commonly used in various bionic robots.[13,39–41] In this work, via utilizing the inherent flexibility of PAMs, we introduce the Netting–Rolling–Splicing (NRS) stacking strategy to quickly and efficiently enable multifunctional soft robots based on the same, simple, and cost-effective structure, as shown in Figures 1 and 2. The NRS robotic stacking not only stacks actuators in 2D to build an actuator net but also involves a step of rolling–splicing to change the topology[42] and raise the soft actuator net from 2D to 3D, rather than directly increasing the stacking dimension to 3D, by which more functions can be achieved than current 2D structures or other 3D stacking strategies (Table 1).

We first employed two types of PAMs, that is, contractile PAMs (CPAM) and wrinkle PAMs (WPAM), as the input to build rectangular cells and 2D programmable cell arrays where mortise-and-tenon joints[14,43] were used for convenient connections. Actuator nets can then be transformed into 3D robots with both sectional and axial "muscles" and inner "tract" in different unit types (including triangle, quadrilateral, and pentagon ones). The sectional "muscles" enable NRS robots to actuate their bodies not only axially but also sectionally, and the inner tract changes the topology of robots and provides an additional interaction surface. This endows them with multimodal interactions and multiple functions

including mono-oscillation crawling, wave crawling, out-pipe/inner-pipe climbing, rotating–climbing, rolling, swallowing/storing/disgorging, and multi-degree-of-freedom (multi-DOF) manipulation, as shown in Figure 1.

To demonstrate the superiority of the NRS method, a TriUnit (the basic or the simplest NRS unit) robot with different WPAM and CPAM arrangements was developed. As a result, the TriUnit robot based on WPAMs can crawl 0.46 ± 0.022 body length per second (BL/s), climb 0.11 BL/s, carry a 3 kg payload while climbing, and achieve omnidirectional pipe crawling, panoramic shooting, and cargo transferring. Several TriUnits were stacked together to conduct bionic wave crawling, robotic swallowing/regurgitating, and multimodal manipulation. The 7-TriUnits robot manipulator with 28 DOFs was able to realize both multi-DOF manipulation and bionic swallowing. The manipulator can not only be used to pick-and-place a payload of 1 kg but also swallow and store objects in its body. A rolling robot based on pentagon unit was also built and able to roll steadily with a speed of 0.19 BL/s.

Main contributions of this work include: (1) the development and implementation of the NRS stacking concept, a new robotic stacking, or topological transformation method that can be used to raise 1D soft actuators to 3D flexible robots; (2) the development of a general analytical and numerical hybrid model, which is able o predict and evaluate the performance behaviors of both WPAMs and normal PAMs in terms of deformability and stiffness variation, thus guiding the programming/reconfiguration of the soft stackable robots; and (3) the design, fabrication, and demonstration of diverse locomotion modes (including crawling, climbing, swallowing, rolling, and manipulation) inspired by living creatures (including worms, monkeys, snakes, spiders, and elephant trunks), based on the same TriUnit. The NRS PAMs based soft stackable robot may bring a new and appealing approach for building multifunctional and multimodal soft robots in a cost-effective and efficient way.

Design and Fabrication

Modeling and characterization of CPAMs and WPAMs

WPAM is a type of extensile PAM (EPAM). The relationship between inner radius and extension ratio usually
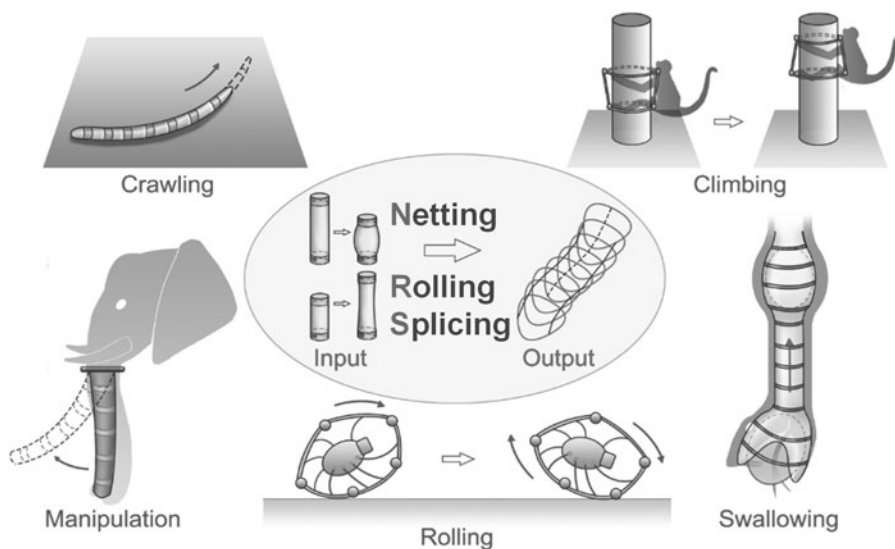

FIG. 1. Multifunctional soft bioinspired robots enabled by the NRS method. NRS, Netting–Rolling–Splicing.
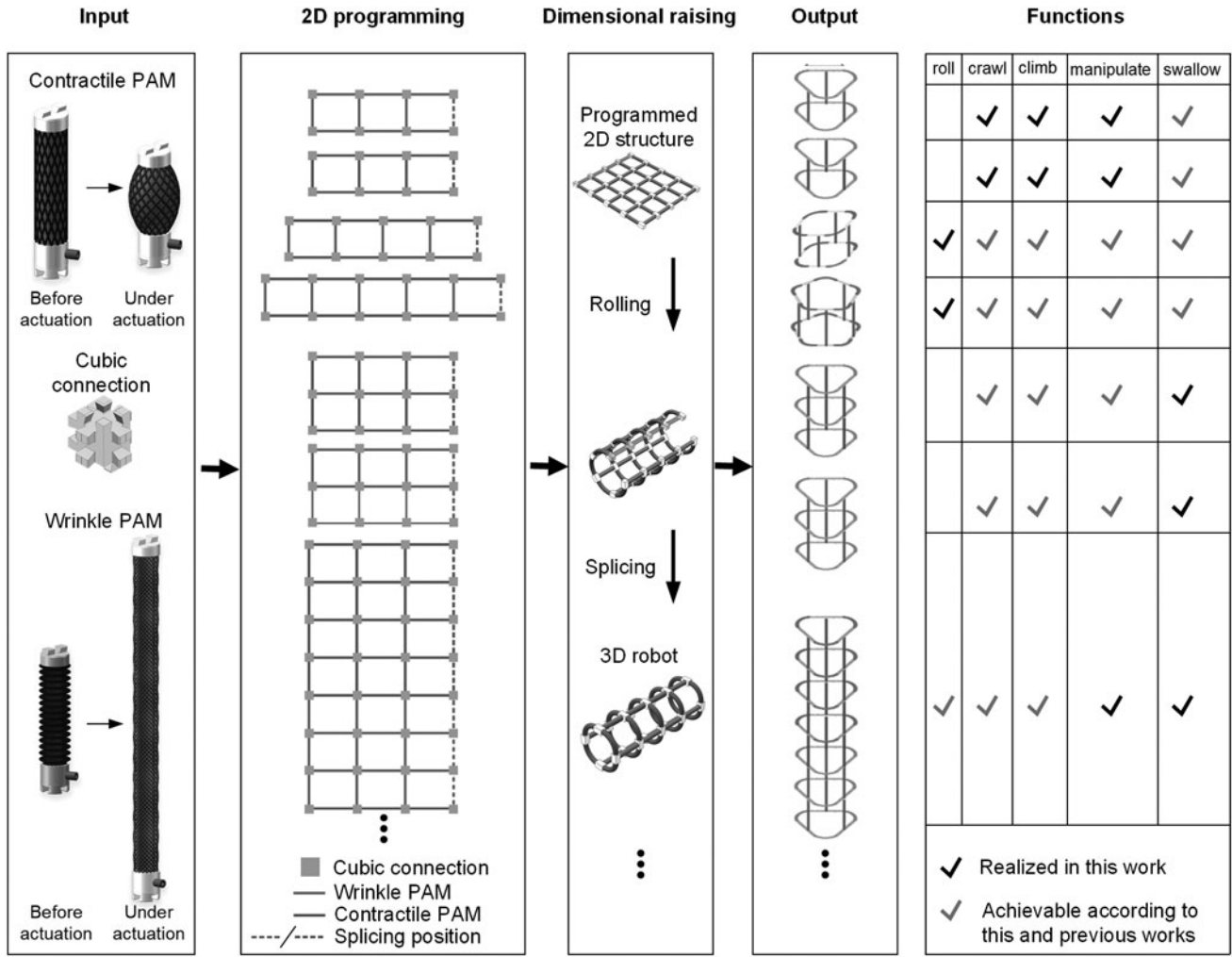
FIG. 2. The NRS design framework for designing soft robots with diverse functions and modalities.

determines the output performance. The inner radius of WPAM, however, increases with the stretch ratio in the start, which is quite different from normal EPAM or CPAM without wrinkles, and can be used to strengthen the output extension force. The parameters of the CPAMs and WPAMs can be seen in Supplementary Table S1. From Figure 3a and Supplementary Figure S2a, contraction displacements of CPAM increased with increasing the pressure, but its contraction displacements and stroke decreased slightly while increasing the load.

For example, under 0 g, the maximum contraction displacement and stroke were both 6.08 ± 0.01 mm under 400 kPa, whereas under 2000 g, they were 4.14 ± 0.02 and 5.60 ± 0.02 mm under 400 kPa, respectively. It should be noted that five tests were repeated here. Extension displacements of WPAM also increased with increasing the pressure (Fig. 3b and Supplementary Fig. S2b), while increasing the load (0–2000 g) increased the extension displacement (66.43–100.3 mm) but decreased the stroke (66.43–18.27 mm) significantly as shown in Figure 3b.

We developed a general analytical and numerical hybrid static model, which is applicable for WPAMs and normal PAMs including CPAMs. Considering the initial gap between the bladder and the braid sleeve, and involving the

Neo-Hookean hyperelastic material model for the bladder material. The output force of the actuator can be expressed as:

$$
F = \begin{cases}
F^*_{\text{air}} + F^*_{\text{bl}} = 2C_1 \left(\lambda_1{}^2 - \frac{1}{\lambda_1{}^2 \lambda_2{}^2} \right) A_{\text{bl}} - PS_{\text{br}}, & \text{uncontacted} \\[2ex]
F^*_{\text{air}} + F^*_{\text{bl}} + F_{\text{br}} = 2C_1 \left(\lambda_1{}^2 - \frac{1}{\lambda_1{}^2 \lambda_2{}^2} \right) A_{\text{bl}} - PS_{\text{br}} \\
\qquad\qquad + (P - P_c) f_{\text{br}}(\lambda_1), & \text{contacted} \\
\text{with } \lambda_1 = \lambda_{1,\text{br}} = \lambda_{1,\text{bl}},
\end{cases}
$$

(1)

where F is the output axial tension force, F^*_{air}, F^*_{bl} are the modified expressions of the forces produced by the air pressure and bladder materials, respectively, F_{br} is the output force from the braid sleeve, C_1 is the material parameter, A_{bl} is the sectional area of the bladder, and $\lambda_{1,\text{bl}}$, $\lambda_{2,\text{bl}}$ are the axial and circular stretch ratios of the bladder, respectively. $\lambda_{1,\text{br}}$ is the axial stretch ratio of the braid sleeve. f_{br} defines the contributed output force of braid sleeve from the effective pressure $P_{\text{effect}} = P - P_c$, and P_c is the critical pressure at which the bladder just starts to contact the inner wall of the braid tube.

According to the test results shown in Supplementary Figure S3c and d, the scale factor of output force to P after the
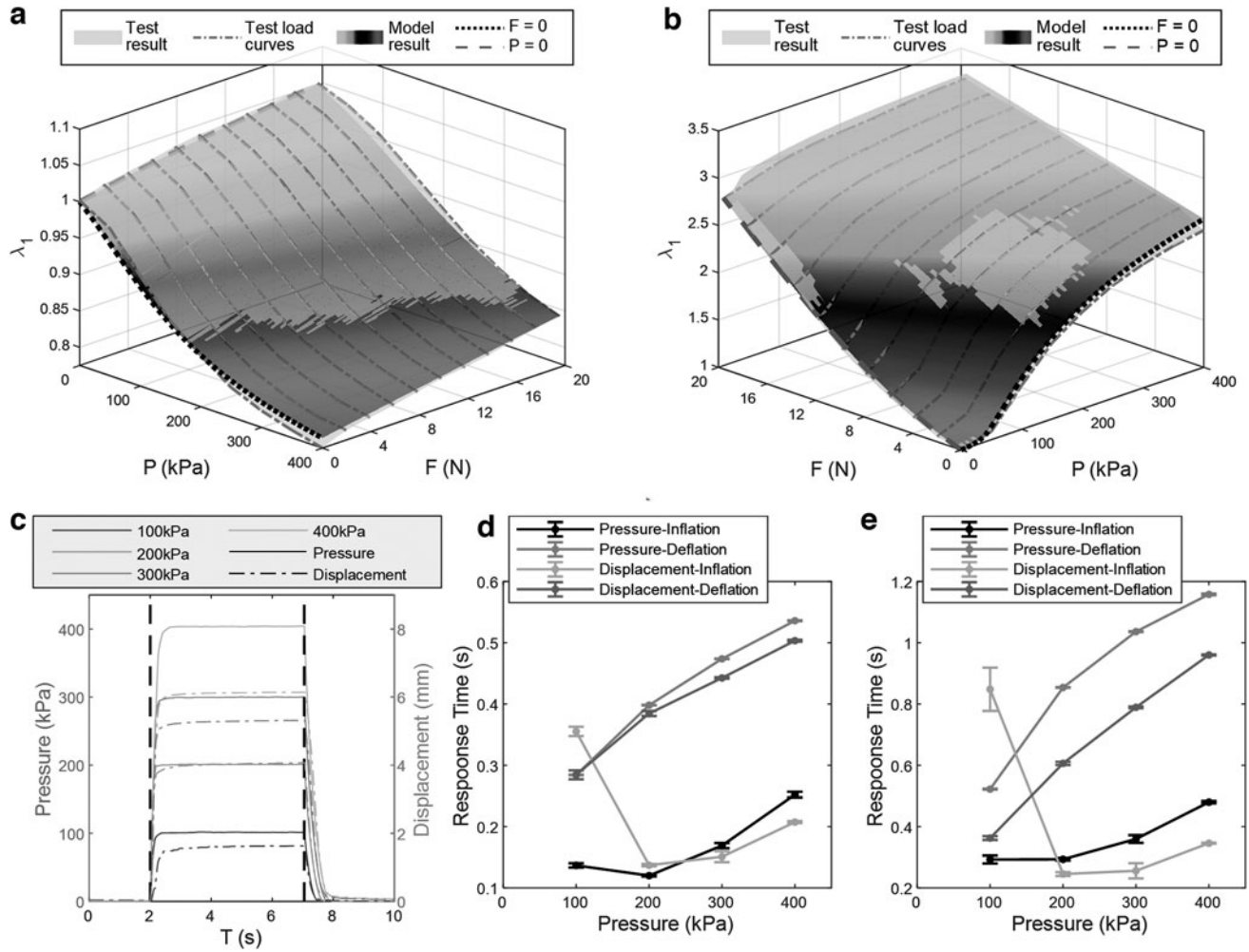
FIG. 3. Static and dynamic performance characterization of the CPAM and WPAM. **(a)** The test and model results of the relationships among stretching ratio λ_1, Pressure P, and bearing load F of the WPAM. **(b)** The test and model results of the relationships among the stretching ratio λ_1, pressure P, and bearing load F of the CPAM. **(c)** Relationship of pressure and displacement to time regarding the CPAM. **(d)** Relationship between pressure and displacement response time and pressure regarding the CPAM. **(e)** Relationship between pressure and displacement response time and pressure regarding the WPAM. CPAM, contractile PAM; PAMs, pneumatic artificial muscles; WPAM, wrinkle PAMs.

contact, $f_{pre}(\lambda_{1,br})$ has a linear relationship with $\lambda_{1,br} = \lambda_1$. Thus, $f_{pre}(\lambda_{1,br})$ can be expressed as a linear function of λ_1 by introducing two parameters k_3 and C_2 as:

$$f_{pre} = \frac{\partial F}{\partial P} = -\frac{dV}{dL} = -S_{br} - L\frac{dS_{br}}{dL}$$
$$= -(k_2L + C_2) = -(k_2L_0\lambda_1 + C_2) = -(k_3\lambda_1 + C_2) \quad (2)$$

Then, the section area of the bladder tube S_{br} and the f_{br} can also be expressed as functions of λ_1.

$$S_{br} = \frac{V_0 + \int_{L_0}^{L} \frac{dV}{dL} dL}{L} = \frac{V_0 + \int_{L_0}^{L}(k_3\lambda_1 + C_2)d\lambda_1 L_0}{L}$$
$$= \frac{V_0}{L} + \frac{\int_{L_0}^{L}(k_3\lambda_1 + C_2)d\lambda_1}{\lambda_1} \quad (3)$$
$$= = \frac{S_{0,br}}{\lambda_1} + \frac{k_3}{2}\lambda_1 + C_2 - \frac{\left(\frac{k_3}{2} + C_2\right)}{\lambda_1},$$

$$f_{br}(\lambda_{1,br}) = -PL\frac{dS_{br}}{dL} = S_{br} - \frac{dV}{dL}$$
$$= \frac{S_{0,br}}{\lambda_1} - \frac{k_3}{2}\lambda_1 - \frac{\left(\frac{k_3}{2} + C_2\right)}{\lambda_1}. \quad (4)$$

Thus, the geometric relationship between the radius and the length can be defined with two geometric parameters C_2 and k_3 numerically based on test results. Then, F_{air}^*, F_{br}, and F_{bl}^* can be derived analytically based on the hyperelastic material constitutive equations[44] and static analysis (see details in the Supplementary Data S1).

With this model, we can draw the output of the WPAM and CPAM with three parameters (C_1, C_2, and k_3) calibrated by the test data, as shown in Figure 3a and b, which is much simpler and more compatible than previous works,[19,45] and can be utilized in their stiffness analysis (including stretching, bending, shear, and torsion stiffness, see details in the Supplementary Data S2). The deviations of the model were 7.21% and 14.71% for the axial load tests of WPAM and the CPAM, respectively. In addition, the model predicted that

both the WPAM and CPAM increased their bending stiffness with raising pressures, whereas CPAM owned higher bending stiffness and wider stiffness range, which can also be verified by the free vibration tests as shown in Supplementary Figure S11.

The relationship between pressure and response time was measured to characterize the dynamic performance using the setup shown in the Supplementary Data S3. Response behaviors of pressure and displacement curves under 100 to 400 kPa can be seen in Figure 3c and Supplementary Figure S12c, where similar hysteresis effects were observed at different pressures (Supplementary Fig. S12a, b). Inflation and deflation response times of the CPAM and WPAM from 10% to 90% pressures and displacements, under different target pressures, can be seen in Figure 3d and e, respectively. During deflation, the pressure and displacement response times of both CPAM and WPAM tend to increase with the target pressure, whereas their response times during inflation at lower target pressure (e.g., $p = 100$ kPa) tend to be higher than that at higher target pressures (e.g., $p = 200$ kPa), especially for the displacement. This may be due to the pressure deadband and the hysteresis effect of the actuator.

Design and fabrication of NRS stackable soft robots

To realize multifunctional and multimodal soft robots in a cost-effective and efficient way, we propose the NRS stacking concept and use it to transform 1D actuators to 3D robots, where the roles of "sectional" and "axial" actuators in the actuation of NRS robots were investigated to provide the basic principles for multimodal and multifunctional robot designs. WPAMs and CPAMs were normal McKibben actuators developed using bladders, braids, and end fittings.[13] In this work, their end fittings were modified by adding the mortise and tenon structures on each end (Fig. 2). Thus, these modular PAMs can be connected with each other via the cubic module with six-direction mortise-and-tenon connections to build 2D actuator nets or 3D robots. Details of the six-direction connection module are added in Figure 2 to better show the mechanisms of the mortise and tenon structure for the plug-and-play connection.

Here, the "Netting" was defined as connecting modular actuators to form a 2D actuator net based on rectangular cells in two perpendicular directions. The "Rolling" was defined as rolling the 2D actuator net in one direction based on the flexibility of PAMs. The "Splicing" was defined as splicing/linking the two end edges of the rolled 2D actuator net to build a 3D actuator structure, as shown in Figure 2. The configuration and function of NRS robots can be programmed in the step of "Netting" by inputting matched actuators, choosing different rectangular cells, and adjusting the cell array arrangement, as shown in Figure 2. By controlling the deformation and stiffness of implemented actuators, the robots can conduct different tasks. And these actuators can be classified into "sectional" and "axial" actuators, which have different roles in the actuation of the robots. For example, the sectional actuators can not only change the sectional scale but also change the cross profile, and the axial actuators can not only vary the axial length but also vary the curvature along the length (Fig. 4).

For sectional actuations, WPAMs have large extension ratios but less stiffness variations, so the sectional size can

not only more than double the origin size (involved in crawling, climbing, and swallowing) but also be able to change its shape by inflating different actuators (involved in rotating–climbing), as shown in Figure 4a(i). However, due to less length changeability but higher stiffness range, even though the sectional CPAMs cannot scale down much and change the shape with triangle configuration, they still can change the sectional profile with variable stiffness (involved in rolling), as shown in Figure 4a(iii).

For the axial actuators, we here show the TriUnit as an example, which has omnidirectional bending and variable stiffness capabilities (involved in manipulation). High stiffness (load bearing of 6 kg) can be achieved using CPAMs, and large bending angles (86°) can be achieved using WPAMs (Fig. 4b and Supplementary Movie S1). Meanwhile, the sectional and axial actuators have some coupled effects on the bending deformation and load-bearing capability.

As can be seen from Figure 4c and d, CPAM and WPAM TriUnit bending angles increased with increasing the axial PAM pressures from 100 to 400 kPa. CPAM TriUnit bending angles increased with the increasing sectional PAM pressures, whereas WPAM TriUnit bending angles decreased with the sectional PAM pressures due to the fact that contraction of the sectional CPAM and extension of the sectional WPAM would decrease/increase the cross-sectional size. The bending angle of the TriUnit is limited to under 90° due to the bucking effect under higher compressing forces when the activated PAMs is further extended. This is because only two ends of each actuator are fastened on the sectional bases. To increase the bending angle range, flexible structures (such as flexible frames or shell sleeves) can be combined with these actuators not only on their ends but also along their lengths.[46,47]

Under low pressures such as 0 and 100 kPa, axial CPAMs of the CPAM TriUnit buckled at certain loads. For example, under 100 kPa, axial CPAMs buckled at 19.2 ± 1.0 N (Fig. 4e). Under higher pressures from 200 to 400 kPa, no buckling was observed due to the increased load capability achieved by the enhanced stiffness under higher pressure. On the contrary, for the WPAM TriUnit, the load capability decreased with increasing the pressure, mainly due to decreased structural stiffness resulting from the increased length–diameter ratio (Fig. 4f). Sectional PAMs also have a large effect on the load capability, as can be seen in Figure 4g, where the inflation of sectional CPAMs increased the structural stiffness and load capability significantly when the axial PAM pressure was at 200 or 400 kPa (involved in manipulation). This was because the torsion stiffness of sectional CPAMs increased with the pressure significantly (Supplementary Fig. S10b), which changed the boundary conditions of the vertical CPAMs from hinge support to fixed support.

Results

In this section, five locomotion modes (crawling, climbing, swallowing, rolling, and manipulation) of NRS-based robots were achieved with different programmed configurations based on the actuation principles described in the Design and Fabrication section. For each locomotion mode, these actuators were divided into several groups according to their actuation roles in bioinspired locomotions and controlled by periodic sequence signals provided by a specific rhythm
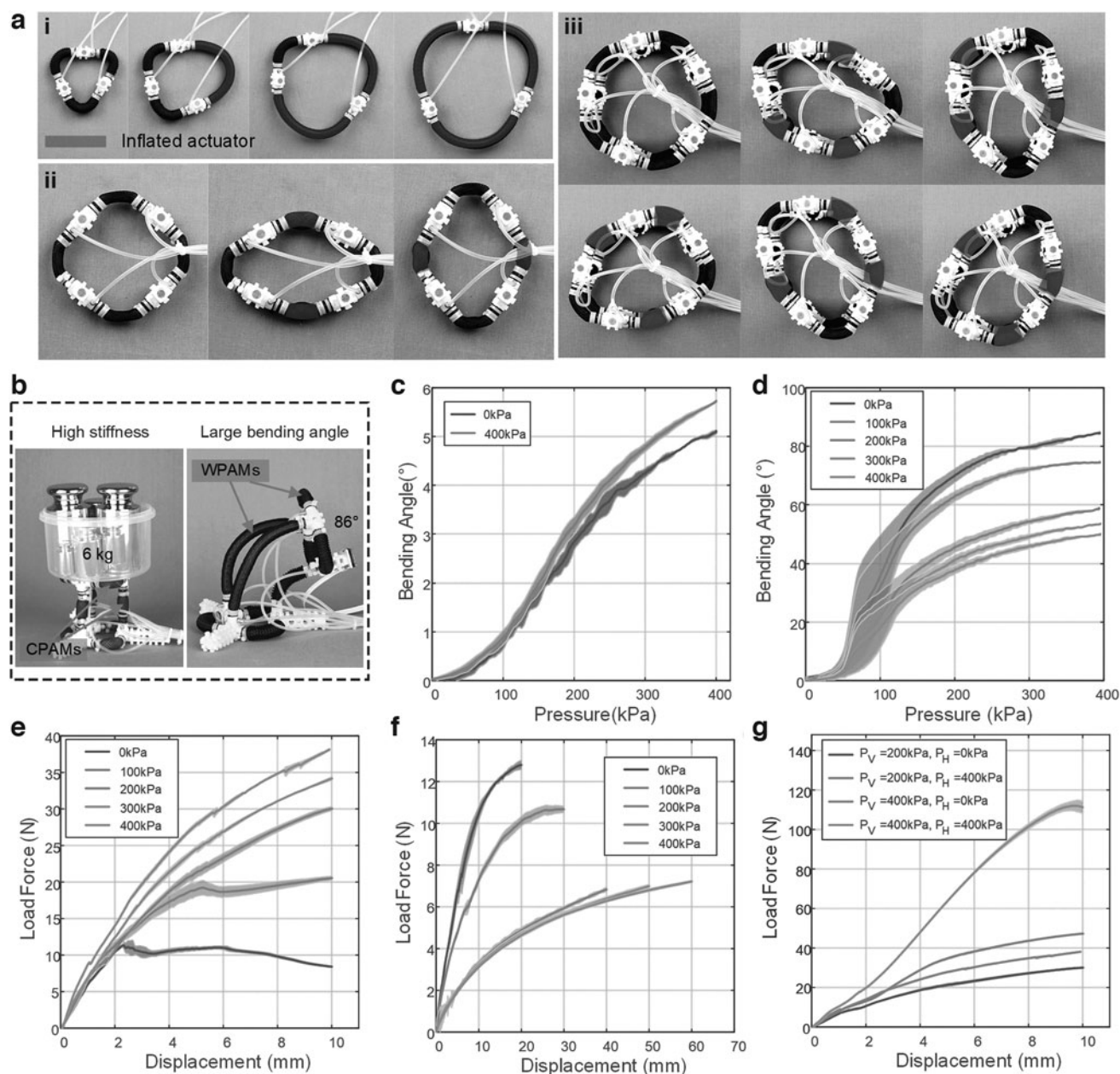
FIG. 4. Sectional and axial actuation of NRS stackable robots based on large deformability and variable stiffness. **(a)** Variable sectional profiles based on length (i: WPAMs) and stiffness changing (ii, iii: CPAMs). **(b)** High stiffness with all CPAMs (supporting 6 kg at 400 kPa) and large bending angle (85°) with all WPAMs of the TriUnits (self-weight of 75 g). **(c)** Relationship between bending angle and the pressure of axial PAMs under different pressures of sectional PAMs regarding the CPAM TriUnit. **(d)** Relationship between bending angle and the pressure of axial PAMs under different pressures of sectional PAMs regarding the WPAM TriUnit. **(e)** Relationship between load and displacement regarding the CPAM TriUnit under different pressures of axial actuators. **(f)** Relationship between load and displacement regarding the WPAM TriUnit under different pressures of axial actuators. **(g)** Relationship between load and displacement regarding the CPAM TriUnit under different pressures of axial (P_V) and sectional (P_H) actuators.

generator. Thus, by tuning the oscillation period, amplitude, and phase difference, different robot locomotion speeds, strides, and patterns can be achieved to perform different tasks.

Mono-oscillation and wave crawling of the TriUnit

Crawling is a basic locomotion function of mobile robots. The TriUnit can also be used for a simple unidirectional

crawling inspired by earthworms.[48] The TriUnit crawler (equipped with one-way wheels) with three axial WPAMs crawled much quicker than the TriUnit with three axial CPAMs due to the larger inflation stroke that can be achieved by WPAMs (Fig. 5a, b and Supplementary Movie S2). The control strategy of the CPAM and WPAM crawler is inspired by the body creeping and feet locating of caterpillar, as shown in Figure 5c, where only the axial actuators were used for crawling.
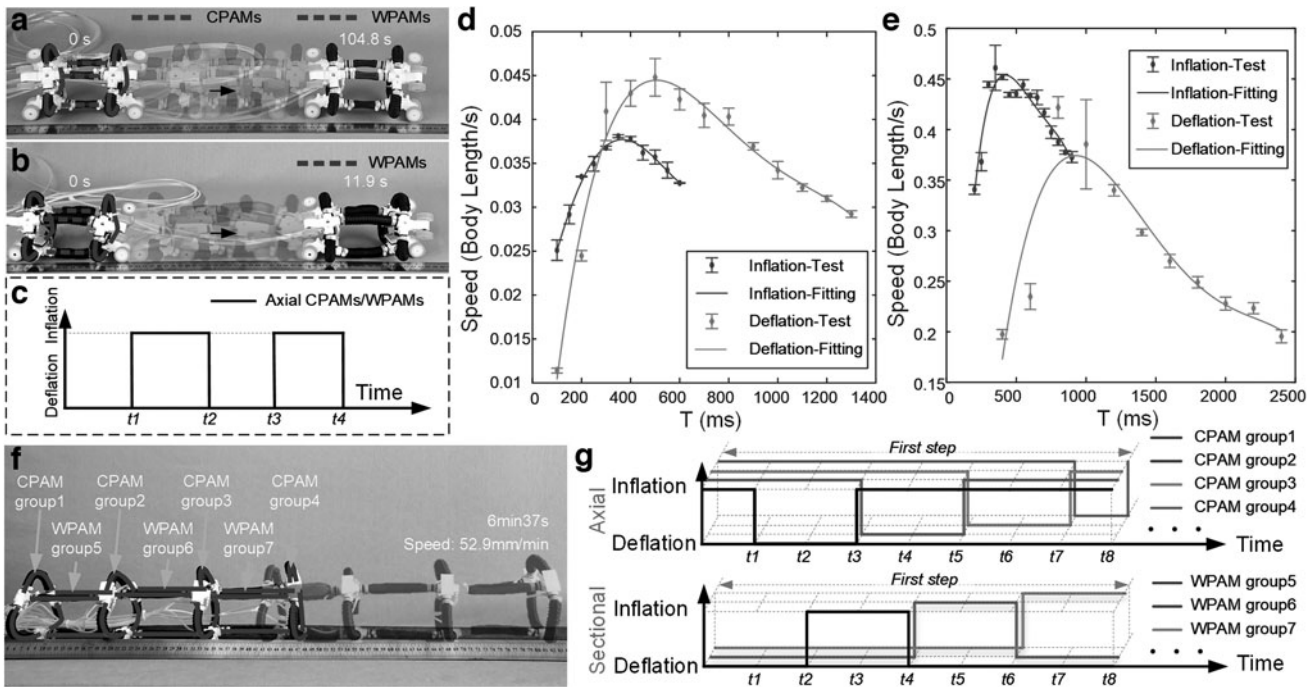
FIG. 5. Crawling performance characterization of the TriUnit. **(a)** Crawling based on the TriUnit with three axial CPAMs and three sectional WPAMs. **(b)** Crawling based on the WPAM TriUnit. **(c)** Control strategy of the CPAM TriUnit-based crawling (the same with WPAM-based crawling). **(d)** Relationship between inflation/deflation time and crawling speed using the CPAM TriUnit. **(e)** Relationship between inflation/deflation time and crawling speed using the WPAM TriUnit. **(f)** Wave crawling based on multiple TriUnits with axial CPAMs and sectional WPAMs. **(g)** Control strategy of the wave crawling.

Crawling speeds of the CPAM TriUnit increased with increasing inflation time and decreased after reaching the maximum speed of 0.038 ± 0.00017 BL/s (inflation time around 0.35 s), when fixing the deflation time of 1 s (Fig. 5d). It also increased with increasing deflation time and decreased after reaching the maximum speed of 0.045 ± 0.0021 BL/s (deflation time around 0.5 s) when fixing the inflation time of 0.5 s. Crawling speeds of the WPAM TriUnit also reached its maximum speed of 0.46 ± 0.022 BL/s with inflation time around 0.50 s when fixing the deflation time of 1.0 s (Fig. 5e). And it reached the maximum speed of 0.42 ± 0.010 BL/s with the deflation time around 1.0 s when fixing the inflation time of 0.5 s (Fig. 5e).

The inflation/deflation times of the maximum speed states for both the CPAM and WPAM TriUnits meet well with the dynamic response time of the actuators as shown in Figure 3d and e, which reveals that dynamic responsive behaviors are non-negligible to obtain the ideal performance of PAM-based soft robots. Larger deviations shown in the crawling with the TriUnit with WPAMs were due to the decreased stability resulted by the reduced structural stiffness of the TriUnit with increase in the length of the axial actuators.

It is worth noting that the wave crawling locomotion inspired by the earthworm can also be realized by stacking multiple TriUnits with no need for one-way structures such as the one-way wheels (Fig. 5f and Supplementary Movie S2), even its speed (1.44 BL/min) was much lower than these crawlers with one-way wheels. This means that the robot can achieve not only forward motions but also backward motions.

Omnidirectional pipe climbing of the TriUnit

Climbing is an unusual locomotion ability of mobile robots so that they move on various 3D wall surfaces to conduct given tasks. The TriUnit can further be used for both out-pipe and in-pipe climbing (with foot pads shown in Fig. 6a, b and g and see Supplementary Fig. S14 and Supplementary Movie S3). The TriUnit with three axial CPAMs (Fig. 6a) climbed much slower than the TriUnit with three axial WPAMs (Fig. 6b). The locomotion of the CPAM and WPAM climbers is based on the movement of releasing, contraction/extension, and embracing, inspired by arm or leg clamping-and-releasing motion of monkeys and can be seen in Figure 6c and d, respectively. The strategy shown in Figure 6c can also be used for the downward climbing of the WPAM climber, and the strategy shown in Figure 6d is also valid for downward climbing of the CPAM climber.

Climbing speeds of the CPAM and WPAM TriUnits increased with increasing the pressure, as shown in Figure 6e, which corresponds to the increasing displacement with the pressure in Figure 3a and b. Climbing speeds of the WPAM TriUnit, however, decreased with increasing carrying loads as shown in Figure 6f, which agrees well with the decreasing stroke under increasing loads as shown in Figure 3b. The maximum payload of the WPAM climber was around 3 kg, even though there was a slight slipping during climbing (Supplementary Movie S3), which was 36 times of its self-weight (83.1 g).

Besides, more locomotion modes can be realized by changing the control strategies. Owing to the compliant body, both
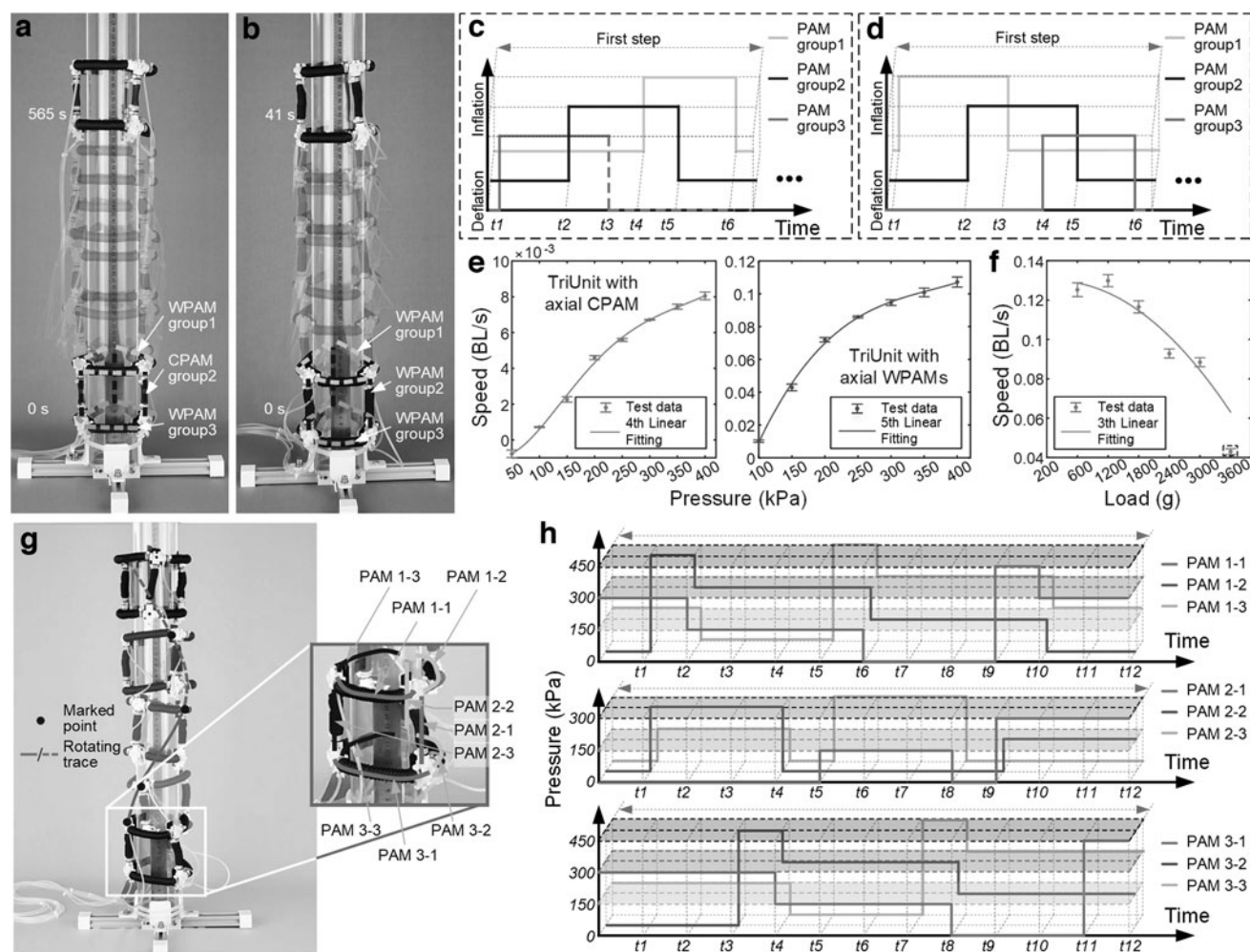
FIG. 6. Climbing performance characterization of the TriUnit. **(a)** Climbing based on the TriUnit with three axial CPAMs and three sectional WPAMs. **(b)** Climbing based on the WPAM TriUnit. **(c)** Control strategy of the CPAM TriUnit-based climbing. **(d)** Control strategy of the WPAM TriUnit-based climbing. **(e)** Relationships between climbing speed and inflation pressure regarding the CPAM TriUnit and the WPAM TriUnit, respectively. **(f)** Relationship between climbing speed and load regarding the WPAM TriUnit. **(g)** Anticlockwise rotating climbing based on the WPAM TriUnit. **(h)** Control strategy of the WPAM TriUnit-based anticlockwise rotating climbing.

TriUnits can be used to achieve in-pipe climbing as shown in Supplementary Figure S14c and d and Supplementary Movie S3. The TriUnit with axial WPAMs can also achieve clockwise and anticlockwise rotation with a speed of 1.6°/s while climbing out of the pipe, as shown in Figure 6g and Figure S14a and b and Supplementary Movie S3. Its rotation motion depends on the independent control of all nine actuators and their unsymmetrical locomotion, inspired by the cooperation of monkey limbs and spine during lateral arboreal movements (Fig. 6h). It is worth mentioning that the TriUnit with axial CPAMs can be used to conduct rotating movements while climbing in the pipe, even though it was owed to the asymmetric huddling under the constraint of the pipe, as shown in Supplementary Movie S3.

Bionic swallowing and regurgitating based on stacked TriUnits

Swallowing is an essential capability of many living creatures for them to take food. Robotic swallowers can be used for useful grasping[32,33] and transporting[34–36] applications. In this work, robotic swallowers based on TriUnits were developed for both enveloping gripping and inner-through transporting. Thus, the robotic swallower can not only achieve swallowing and storing but also for animal-like regurgitating and inner material transportation. For better visualization, we stacked three TriUnits together to form a vertical robotic swallower, where two TriUnits were based on both WPAMs and CPAMs, and one TriUnit was based on WPAMs. A 3D printed ball with a diameter of 120 mm and weight of 89 g was vertically swallowed by the robotic swallower (Fig. 7a and Supplementary Movie S4). The swallowing behaviors were realized by the continuous squeezing and pushing of the sectional and axial PAMs, inspired by the snake swallowing and achieved by sequential inflation and deflation of PAM groups 1–6, as shown in Figure 7c.

We also tested a robotic swallower with three TriUnits based on all WPAMs. With WPAMs as axial PAMs instead of CPAMs, the swallower achieved larger work spaces as shown in Supplementary Movie S4, but due to the larger
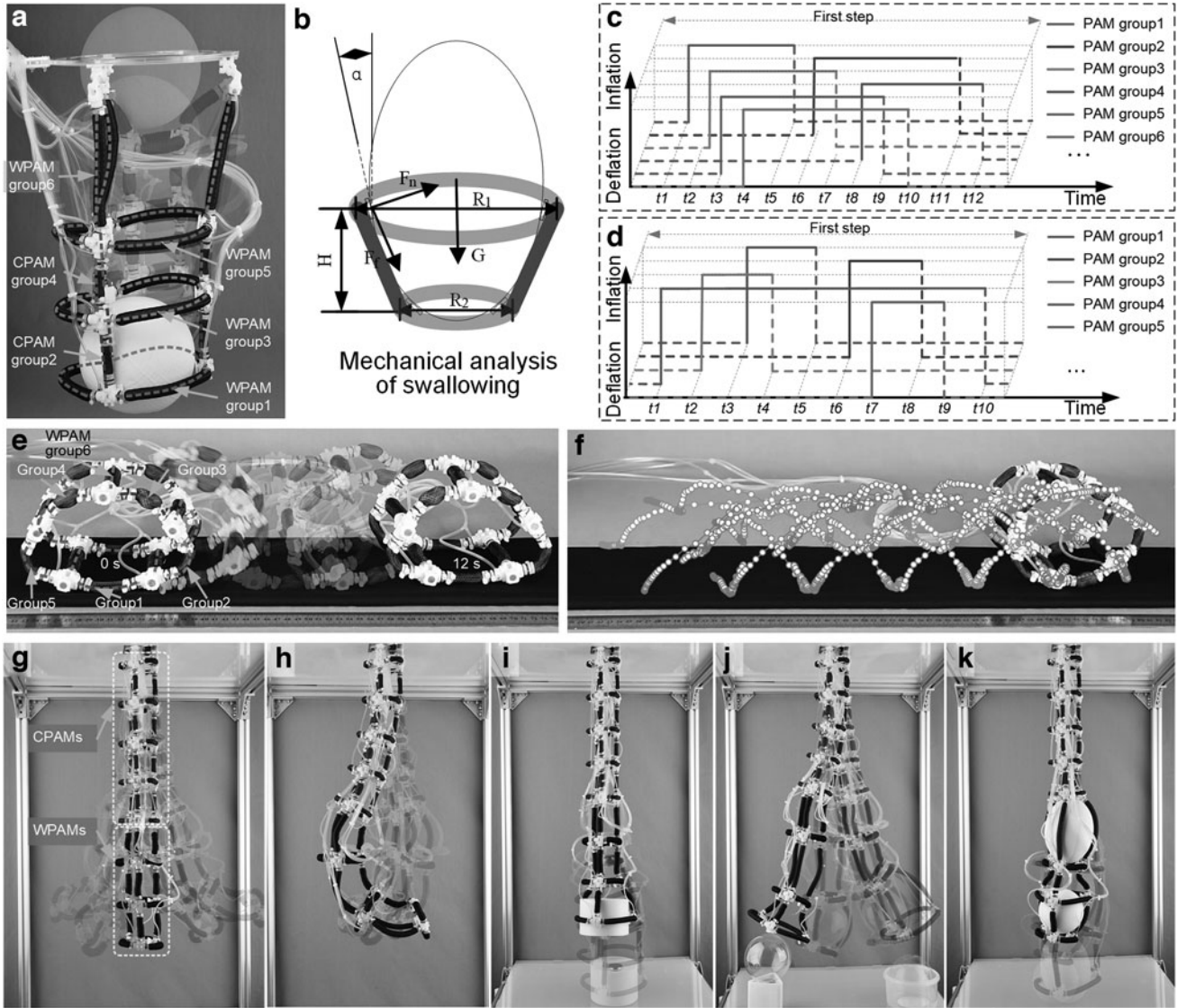
FIG. 7. Demonstration of robotic swallowing, rolling, and multimodal bending and manipulation. **(a)** Swallowing of a 3D printed ball (89 g) based on a combination of CPAMs and WPAMs. **(b)** Mechanical analysis for the swallowing behavior based on the TriUnit, in which G is the gravity of the object and R_1 is the maximum diameter. **(c)** Control strategy of the swallowing process. **(d)** Control strategy of the rolling process. **(e)** Static and stable rolling based on CPAMs of variable stiffness. **(f)** Trajectories of the five connection joints regarding the PenUnit robotic roller. **(g)** Omnidirectional bending. **(h)** Complex trajectory bending. **(i)** Vertical gripping a payload of 1 kg. **(j)** Pick-and-place of a transparent plastic ball (70 g) with a 7-Unit manipulation arm. **(k)** Vertical swallowing and transporting a 3D printed ellipsoid (125 g) and a 3D printed spheroid (89 g).

minimum distance between the two adjacent sections, the swallower with all WPAMs can only swallow and transport the oval ball with larger heights. This was because sectional size and length between each TriUnit are two dominant factors influencing the swallowing performance. From Figure 7b, the condition under which objects can be swallowed and transmitted successfully can be written as below:

$$\sin\alpha \, F_n > \frac{G}{3} + \mu_{st}\cos\alpha \, F_n, \qquad (5)$$

This means that when $R_2 = R_{\min}$, the contact angle α needs to meet the following condition:

$$\alpha > \sin^{-1}\left[\frac{G}{3\,F_n}\left(\sqrt{1+\mu_{st^2}}\right)\right] + \sin^{-1}\left(\frac{\mu_{st}}{\sqrt{1+\mu_{st^2}}}\right) > 0, \quad (6)$$

where μ_{st} is the static friction coefficient of the contact surface, G is the gravity of the object, and F_n is the normal contact force.

It can be concluded that (1) the minimum distance between each TriUnit should be at least less than half the height of the objects, and (2) both ends of the objects need to be as rounded as possible.

Wheel rolling of the PenUnit from lateral stacking

Rolling is a scarce locomotion ability in animals. Stacking multiple omnidirectional bending units (e.g., TriUnits) can be used for vertical rolling gait.[3] But with only one unit, rolling would become much more challenging as the robot needs a large change of gravity center. To achieve that, lateral stacking of the initial 2D actuator net was involved in the

design of the unit, instead of axial stacking. First, the NRS unit based on the quadrilateral cell (abbreviated as QuadUnit) was tested. The QuadUnit has one shape degree of freedom, and the changing range of the center of gravity can meet the requirement of rolling. But its symmetrical structure makes the rolling behavior more random, which limits the controllability of the rolling (Supplementary Movie S5) and makes it only applicable for dynamic rolling[49,50] instead of a static rolling.

The pentagon cell based on an NRS unit (abbreviated as PenUnit) was adopted here for robotic rolling as it has two shape degrees of freedom, which is more complex but has higher controllability. Static stable rolling with a speed of 0.28 BL/s was achieved by the PenUnit as shown in Figure 7e and f, where five sectional CPAM groups were used. The rolling locomotion was inspired by the wheel spider and depended on the sectional profile transforming, and as realized by the sequential stiffness changing of five CPAM groups inflated and deflated in sequence, as shown in Figure 7d. Trajectories of the five connection joints, measured by OpenCV with five color marks, can be seen in Figure 7f. It should be noted that the roll speed is limited by the static gait used in the paper and the response ability of the actuator. To increase the rolling speed, dynamic gaits can be applied to reduce the step time and more efficiently utilize the input energy, and higher air pressures can be used to provide higher flow capacities.

Multi-DOF and multimodal manipulation based on stacked TriUnits

Inspired by the dexterous manipulation capability of elephant trunks and swallowing ability of snakes, we stacked four TriUnits based on CPAMs (to enable large enough bending angle range and load carrying capability) and three TriUnits based on WPAMs (to enable decent swallowing and

gripping) together. As a result, the NRS soft robotic manipulator has a high flexibility of manipulation and owes 28 DOFs (21 degrees for axial PAMs and 7 degrees for sectional PAM groups). Thus, the manipulator can not only achieve simple omnidirectional curvature bending (Fig. 7g) and complex trajectory bending (Fig. 7h) but also be able to realize that multimodal manipulation includes gripping, transporting, swallowing, and storing, as shown in Figure 7i–k.

The NRS soft robotic manipulator was shown to grip a payload of 1 kg placed in a 3D printed hollowed cylinder (82 g, outer diameter of 130 mm, and height of 90 mm), as shown in Figure 7i. The manipulator was also demonstrated to complete pick-and-place of a transparent plastic ball (70 g, diameter of 120 mm), as shown in Figure 7j and Supplementary Movie S6. Moreover, simultaneous swallowing, transporting, and storing materials can also be achieved like snakes. For instance, a 3D printed sphere ball (125 g, 130×180 mm) was swallowed, transported, and stored inside the body, and then, a 3D printed ball (89 g, diameter of 120 mm) was gripped and swallowed continuously (Fig. 7k and Supplementary Movie S6).

Demonstration of panoramic shooting and cargo transferring

Here, we present two task scenarios using the TriUnit robots to demonstrate their potential uses. In the first scenario, we presented an omnidirectional pipe climbing robot carrying a camera (40 g) to explore the surroundings around the pipe. For normal pipe climbing robots, multiple cameras or other structures would be required to cover the view of all angles. Our design can rotate (clockwise/anticlockwise) and climb (up/down) easily to cover the view in every angle and height, as shown in Figure 8a–c and Supplementary Movie S7. In the second task, we present a climbing robot transferring cargos by attaching helical WPAMs as the tentacles.
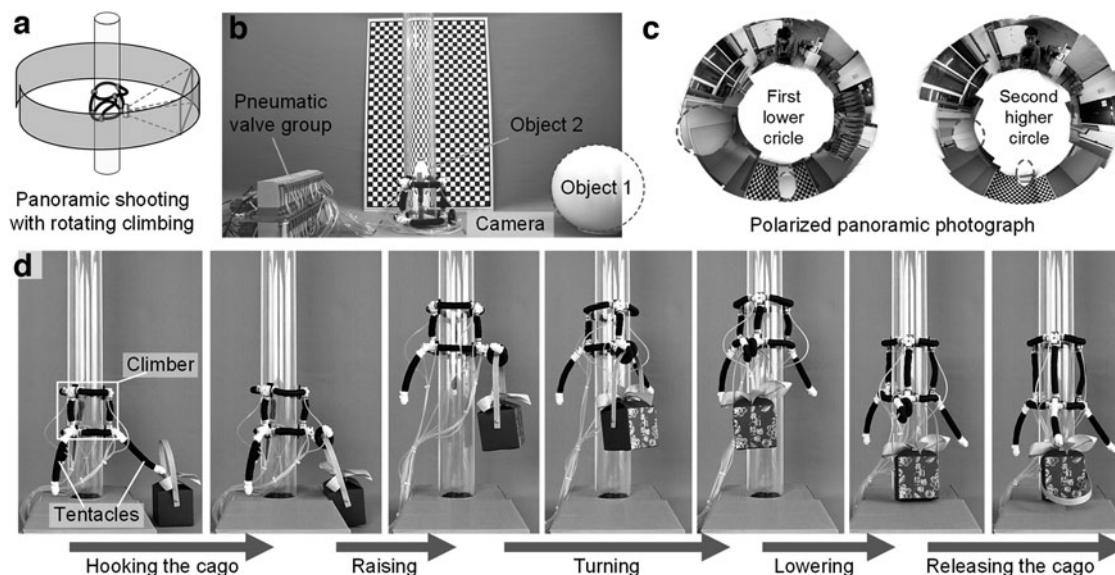

FIG. 8. Demonstration of panoramic shooting and cargo transferring with TriUnit robots. **(a)** The diagram of rotating–climbing-based panoramic shooting. **(b)** The scenery and setting of the panoramic shooting test. **(c)** Polarized panoramic photos in the first (left) and second (right) rotating circle. **(d)** Cargo transferring by the TriUnit robot with tentacles based on helical PAMs.

The robot hooked the cargo (153 g) actively, climbed up to lift the cargo, rotated to the other direction, climbed down, and released the cargo on a higher platform. Owe to the omnidirectional pipe climbing and the soft ''tentacles,'' the pipe climber can transfer cargo in any height and direction around the pipe (Fig. 8d and Supplementary Movie S8).

The two task scenarios not only show the potential applications of the TriUnit robots but also demonstrate that these stackable robots based on PAMs are adjustable for different tasks owing to its modular and soft design. For the demonstration of panoramic shooting and cargo transferring, we aimed to only show the applications of our NRS PAM concept, instead of demonstrating the load bearing or gripping capability of the TriUnit (as showcased in Fig. 7(i) and Supplementary Movies S3 and S6). Nevertheless, greater load capability and gripping forces of both the TriUnit and ''tentacle'' can be achieved by adopting larger actuator diameters.

Discussion

Soft robots equipped with multiple functionalities have been increasingly needed for various tasks in unknown and unpredictable environments. In this work, we have proposed an enabling robotic stacking methodology, NRS, to design and fabricate modular soft robots with various functions by stacking via convenient plug-and-play mortise and tenon joints. We have introduced the concept of actuator input, cell, cell array, dimension raising, and robotic unit output to assist the design of diverse robots with different features.

With the 2D programming and dimension raising process, the input of only two types of actuators was able to produce 3D robots with diverse functions including mono-oscillation crawling, wave crawling, out-pipe/inner-pipe climbing,

rotating–climbing, rolling, swallowing/storing/disgorging, and multi-DOF manipulation. Furthermore, we have developed a general analytical and numerical hybrid model to depict behaviors of both WPAMs and normal CPAMs, including their stretching, bending, shear, and torsion stiffness properties. We have found that the stiffness properties of the input actuators have a significant effect on the performance of the output robots, thus providing useful insights for designing multifunctional soft pneumatic robots.

In Table 1, we have shown that the NRS enabled soft robot, to the best of the authors' knowledge, has the most comprehensive functions, compared with existing stackable soft robots. We have quantitatively compared these robots, as shown in Figure 9, in terms of crawling speed, climbing speed, climbing load capability, rolling speed, bending angle, bending dimension index, inner-through transportation, and enveloping gripping. It is clear that the proposed robot has the best overall robotic performance, which demonstrates the superiority of the NRS method. In addition, panoramic shooting and cargo transferring using the TriUnit robot have further demonstrate the excellent adjustability that is needed for tasks that may find their uses in unstructured and unknown environments.

Deformability and variable stiffness are two intrinsic properties of soft tissues, which endow living creatures with excellent adaptability. Our WPAMs and CPAMs own large deformability and have variable stiffness capabilities that can match the actuation requirement of bioinspired robots. To get better performance, these actuators can be fabricated with select parameters based on the proposed general model for WPAM and CPAM to meet the requirement of deformability or stiffness. According Equations (1), (3) and (4), $S_{br}(\lambda_{1,br})$ dominates the output of PAM. For example, the theoretic extension ratio limit λ_{lim} without bladder effect is determined
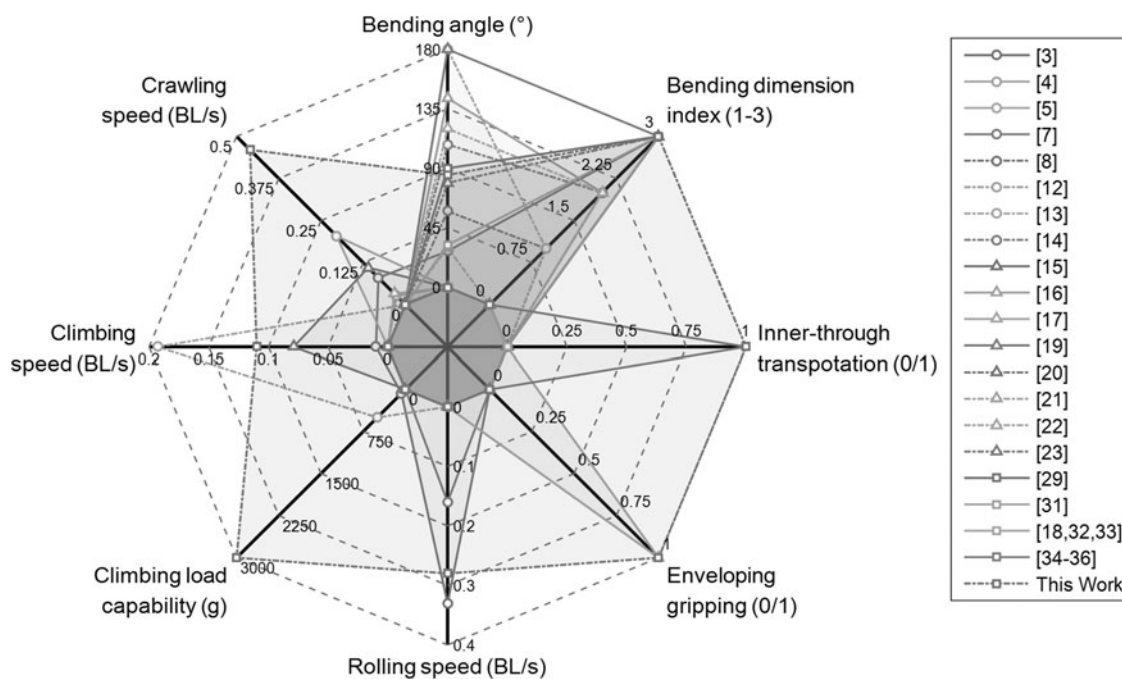

FIG. 9. Quantitative comparison of different multifunctional soft robots with this work, where for enveloping gripping and inner-through transportation, 0 represents unavailable and 1 represents available, and for the bending dimension index, 1 denotes unidirectional, 2 denotes bidirectional, and 3 denotes omnidirectional.

by $f_{pre}(\lambda_{1,br}) = -S_{br} - \lambda_{1,br}\frac{dS_{br}}{d\lambda_{1,br}} = 0$. Thus, to get higher deformability, the design parameters (including wrinkle radius, density, braid angle, and others) could be selected to get as high $|\Delta\lambda_{lim}|$ as possible. When $\Delta\lambda_{lim}>0$, $\Delta|\lambda_{lim}|$ is maximum theoretical contraction ratio limit, and when $\Delta\lambda_{lim}<0$, $\Delta|\lambda_{lim}|$ is the theoretical extension ratio limit.

According to Equation S(46), the bending stiffness of the actuator without bladder effect is also related to the axial force output, $\frac{\partial F_{br}(\lambda_1,P)}{\partial\lambda_1} = P_{effect}\frac{df_{br}}{d\lambda_1}$. Thus, higher bending stiffness could be achieved by increasing the air pressure or choosing the design parameters with high value of $\left|\frac{df_{br}}{d\lambda_1}\right|_{\lambda_1 = \lambda_{free}}$, where λ_{free} is the stretch ratio at free state. It has to be noted that the influence of these actuator design parameter on actuator output was not investigated intensively in this work, instead this model is focused in providing a convenient methodology to evaluate the overall output behavior with a simple axial loading test.

Future work may include but not limited to the following aspects: (1) the inclusion of skeletons and variable stiffness structures to further enhance the loading capability of the aforesaid soft robots; (2) the investigation into other cell types such as hexagon ones and dimension raising methods such as multidirection rolling, staggered stacking, and their combinations, to create more complex robotic configurations; (3) the exploration of other locomotion modes such as swimming in water, burrowing in sands, and sliding on the snow; (4) soft sensors can be integrated onto to the robot to bring proprioceptive and exteroceptive capabilities, and central pattern generators and model-based control methods can be involved with these soft sensors to bring more autonomous and adaptive robots.

Authors' Contributions

J.L. conceived the research. Q.G., L.L., and J.S. designed and fabricated the PAM actuators, modularized robots, and the pneumatic control system. Q.G. and J.W. designed and performed all the experiments, and processed and analyzed the data. Q.G., Y.L., and J.L. interpreted the data and discussed the results. Q.G. and J.G. wrote the article. Q.G. and J.G. jointly proposed the robotic stacking and NRS concept. Y.L. and J.L. directed the research and fully revised the article.

Author Disclosure Statement

No competing financial interests exist.

Funding Information

Supplementary Material

Supplementary Data
Supplementary Movie S1
Supplementary Movie S2
Supplementary Movie S3
Supplementary Movie S4
Supplementary Movie S5
Supplementary Movie S6
Supplementary Movie S7
Supplementary Movie S8

References

1. Zou J, Feng M, Ding N, et al. Muscle-fiber array inspired, multiple-mode, pneumatic artificial muscles through planar design and one-step rolling fabrication. Natl Sci Rev 2021; 8:nwab048.

2. Hu W, Lum GZ, Mastrangeli M, et al. Small-scale soft-bodied robot with multimodal locomotion. Nature 2018; 554:81–85.

3. Robertson MA, Paik J. New soft robots really suck: vacuum-powered systems empower diverse capabilities. Sci Robot 2017;2:eaan6357.

4. Paschal T, Bell MA, Sperry J, et al. Design, fabrication, and characterization of an untethered amphibious sea urchin-inspired robot. IEEE Robot Autom Lett 2019;4:3348–3354.

5. Shepherd RF, Ilievski F, Choi W, et al. Multigait soft robot. Proc Natl Acad Sci USA 2011;108:20400–20403.

6. Mao S, Dong E, Jin H, et al. Gait study and pattern generation of a starfish-like soft robot with flexible rays actuated by SMAs. J Bionic Eng 2014;11:400–411.

7. Marchese AD, Onal CD, Rus D. Soft robot actuators using energy-efficient valves controlled by electropermanent magnets. In: 2011 IEEE/RSJ International Conference on Intelligent Robots and Systems (IROS). San Francisco, CA: IEEE, 2011, pp. 756–761.

8. Stokes AA, Shepherd RF, Morin SA, et al. A hybrid combining hard and soft robots. Soft Robot 2014;1:70–74.

9. Truby RL, Wehner M, Grosskopf AK, et al. Soft somato-sensitive actuators via embedded 3D printing. Adv Mater 2018;30:1706383.

10. Zhang H, Kumar AS, Chen F, et al. Topology optimized multimaterial soft fingers for applications on grippers, rehabilitation, and artificial hands. IEEE ASME Trans Mechatron 2018;24:120–131.

11. Pfeil S, Henke M, Katzer K, et al. A worm-like biomimetic crawling robot based on cylindrical dielectric elastomer actuators. Front Robot AI 2020;7:9.

12. Liao B, Zang H, Chen M, et al. Soft rod-climbing robot inspired by winding locomotion of snake. Soft Robot 2020; 7:500–511.

13. Guan Q, Sun J, Liu Y, et al. Novel bending and helical extensile/contractile pneumatic artificial muscles inspired by elephant trunk. Soft Robot 2020;7:597–614.

14. Kurumaya S, Phillips BT, Becker KP, et al. A modular soft robotic wrist for underwater manipulation. Soft Robot 2018;5:399–409.

15. Zhang Y, Yang D, Yan P, et al. Inchworm inspired multi-modal soft robots with crawling, climbing, and transitioning locomotion. IEEE Trans Robot 2021;38(3):1806–1819.

16. Marchese AD, Katzschmann RK, Rus D. Whole arm planning for a soft and highly compliant 2d robotic manipulator. In: 2014 IEEE/RSJ International Conference on Intelligent Robots and Systems (IROS). Chicago, IL: IEEE, 2014, pp. 554–560.

17. Zou J, Lin Y, Ji C, et al. A reconfigurable omnidirectional soft robot based on caterpillar locomotion. Soft Robot 2018;5:164–174.

18. Hao Y, Biswas S, Hawkes EW, et al. A multimodal, enveloping soft gripper: shape conformation, bioinspired adhesion, and expansion-driven suction. IEEE Trans Robot 2020;37:350–362.

19. Fu HC, Ho JDL, Lee KH, et al. Interfacing soft and hard: a spring reinforced actuator. Soft Robot 2020;7:44–58.

20. Kalisky T, Wang Y, Shih B, et al. Differential pressure control of 3D printed soft fluidic actuators. In: 2017 IEEE/RSJ International Conference on Intelligent Robots and Systems (IROS). Vancouver, Canada: IEEE, 2017, pp. 6207–6213.

21. Li S, Awale SA, Bacher KE, et al. Scaling up soft Robotics: a meter-scale, modular, and reconfigurable soft robotic system. Soft Robot 2022;9(2):324–336.

22. Li S, Vogt DM, Rus D, et al. Fluid-driven origami-inspired artificial muscles. Proc Natl Acad Sci USA 2017;114: 13132–13137.

23. Sui X, Cai H, Bie D, et al. Automatic generation of locomotion patterns for soft modular reconfigurable robots. Appl Sci 2020;10:294.

24. Kopic C, Gohlke K. InflatiBits: A modular soft robotic construction kit for children. In: Proceedings of the TEI 2016: Tenth International Conference on Tangible, Embedded, and Embodied Interaction. New York, NY, United States: ACM, 2016, pp. 723–728.

25. Usevitch NS, Hammond ZM, Schwager M, et al. An untethered isoperimetric soft robot. Sci Robot 2020;5: eaaz0492.

26. Kimber J, Ji Z, Petridou A, et al. Low-cost wireless modular soft tensegrity robots. In: 2019 2nd IEEE International Conference on Soft Robotics (RoboSoft). Seoul, Korea (South), IEEE, 2019, pp. 88–93.

27. Bell MA, Gorissen B, Bertoldi K, et al. A modular and self-contained fluidic engine for soft actuators. Adv Intell Syst 2021:2100094.

28. Patterson ZJ, Sabelhaus AP, Chin K, et al. An untethered brittle star-inspired soft robot for closed-Loop underwater locomotion. In: 2020 IEEE/RSJ International Conference on Intelligent Robots and Systems (IROS). Las Vegas, NV: IEEE, 2020, pp. 8758–8764.

29. Fei Y, Wang J, Pang W. A novel fabric-based versatile and stiffness-tunable soft gripper integrating soft pneumatic fingers and wrist. Soft Robot 2019;6:1–20.

30. Mahl T, Hildebrandt A, Sawodny O. A variable curvature continuum kinematics for kinematic control of the bionic handling assistant. IEEE Trans Robot 2014;30:1–15.

31. Meng C, Xu W, Li H, et al. A new design of cellular soft continuum manipulator based on beehive-inspired modular structure. Int J Adv Robot Syst 2017;14: 1729881417707380.

32. Sui D, Zhu Y, Zhao S, et al. A bioinspired soft swallowing gripper for universal adaptable grasping. Soft Robot 2020.

33. Li H, Yao J, Liu C, et al. A bioinspired soft swallowing robot based on compliant guiding structure. Soft Robot 2020;7:491–499.

34. Chen F-J, Dirven S, Xu W, et al. Design and fabrication of a soft actuator for a swallowing robot. In: Robot Intelligence Technology and Applications 2. Cham: Springer, 2014, pp. 483–493.

35. Zhu M, Xu W, Cheng LK. Esophageal peristaltic control of a soft-bodied swallowing robot by the central pattern generator. IEEE ASME Trans Mechatron 2016;22:91–98.

36. Dirven S, Xu W, Cheng LK, et al. Soft-robotic peristaltic pumping inspired by esophageal swallowing in man. In: Robot Intelligence Technology and Applications 2. Cham: Springer, 2014, pp. 473–482.

37. Wang H, Xu H, Yu F, et al. Modeling and experiments on the swallowing and disgorging characteristics of an underwater continuum manipulator. In: 2020 IEEE International Conference on Robotics and Automation (ICRA). Paris, France: IEEE, 2020, pp. 2946–2952.

38. Zhang Y, Qian Z, Huang H, et al. A snake-inspired swallowing robot based on Hoberman's linkages. J Mech Robot 2022;14:065001.

39. Ohta P, Valle L, King J, et al. Design of a lightweight soft robotic arm using pneumatic artificial muscles and inflatable sleeves. Soft Robot 2018;5:204–215.

40. Gorissen B, Reynaerts D, Konishi S, et al. Elastic inflatable actuators for soft robotic applications. Adv Mater 2017;29: 1604977.

41. Guan Q, Sun J, Liu Y, et al. Status of and trends in soft pneumatic robotics. Sci Sin Technol 2020;50:897–934.

42. Freeman C, Maynard M, Vikas VJSR. Topology and morphology design of spherically reconfigurable homogeneous modular soft robots. Soft Robot 2023;10(1):52–65.

43. Li Y, Zhang Q, Hong Y, et al. 3D transformable modular kirigami based programmable metamaterials. Adv Funct Mater 2021;31:2105641.

44. Guan Q, Sun J, Liu Y, et al. Characterization and nonlinear models of bending extensile/contractile pneumatic artificial muscles. Smart Mater Struct 2021;30:025024.

45. Yukisawa T, Ishii Y, Nishikawa S, et al. Modeling of extensible pneumatic actuator with bellows (EPAB) for continuum arm. In: 2017 IEEE International Conference on Robotics and Biomimetics (ROBIO). Macau, Macao, IEEE, 2017, pp. 2303–2308.

46. Wan Z, Sun Y, Qin Y, et al. Design, analysis, and real-time simulation of a 3D soft robotic snake. Soft Robot 2022. [Epub ahead of print]; DOI: 10.1089/soro.2021.0144.

47. Mcmahan W, Chitrakaran V, Csencsits M, et al. Field trials and testing of the OctArm continuum manipulator. In: IEEE International Conference on Robotics and Automation (ICRA). Orlando, FL: IEEE, 2006, pp. 2336–2341.

48. Zhan X, Fang H, Xu J, et al. Planar locomotion of earthworm-like metameric robots. Int J Robot Res 2019;38: 1751–1774.

49. Puopolo MG, Jacob JD, Gabino E. Locomotion of a cylindrical rolling robot with a shape changing outer surface. Robotics 2018;7:52.

50. Puopolo MG, Jacob JD. Velocity control of a cylindrical rolling robot by shape changing. Adv Robot 2016;30:1484–1494.

Address correspondence to:
Jinsong Leng
Centre for Composite Materials and Structures
Harbin Institute of Technology (HIT)
No 2 Yikuang Street
Harbin 150080
People's Republic of China

E-mail: lengjs@hit.edu.cn